# Chapter 3

## *Carbon nanotube (CNT) embedded cyclodextrin polymer derived injectable nanocarrier: A multiple faceted platform for stimulation of multi-drug resistance reversal*

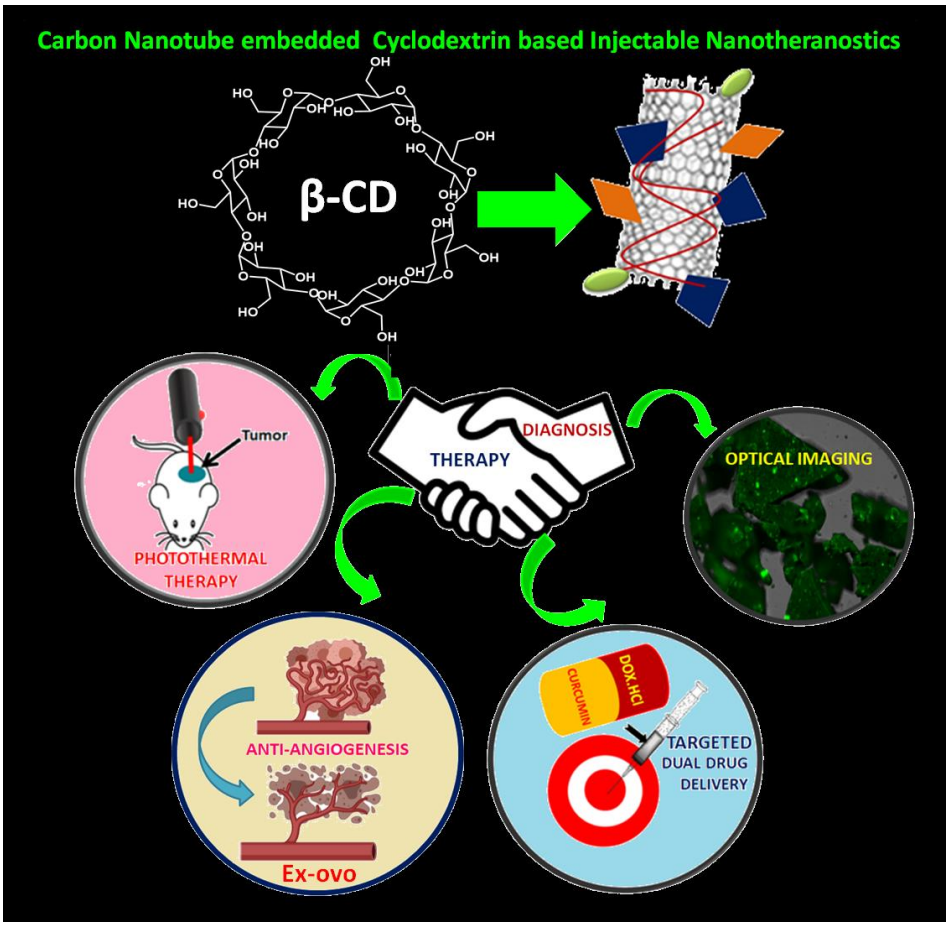


**Published in *Carbohydrate Polymers*, 2020, *247*, 116751-116763**

### 3.1 Introduction

Cancer therapy has shown a significant improvement over past decades with more effective drugs and better safety profiles. Despite these improvements unwanted side effects arising due to dearth of selectivity in conventional chemotherapy is an enigma which needs to be addressed [1,2]. Deploying nanosized drug loaded cargos for cancer management provides an upper hand by improving stability and solubility of drug molecules [3], eluded drug release at normal tissues by their interaction with desired functional groups [4] and most importantly targeting tumors by response to cancer specific stimulus [5]. Recent treatment strategies involve combining different modalities like single/multiple drug based chemotherapy, radiotherapy, hyperthermia by modulating substrates like gold [6], mesoporous silica [7], polymer nanoparticles[8], graphene [9], carbon nanotubes [10] etc. to design drug carriers for more efficacious cancer management [11]. However there are several repercussions associated with these modalities including severe systemic toxicity, low specificity and drug resistance limiting multidrug resistance (MDR) their clinical applications [12]. Tables 3.1-3.3 give the state of art in materials developed for cancer therapy.

**Table 3.1: CNT derived therapeutics/theranostics**

| System | Salient Features | References |
|---|---|---|
| RuPOP@MWCNTs (Ru polypyridyl complex derived MWCNTs) | Enhanced anticancer efficacy by multidrug resistance and radio-resistance | [18] |
| Biopolymer conjugated CNTs loaded with DOX MWCNTs/DOX/TC | Chemo-photothermal combination therapy | [13,19] |
| Polymer derived MCNTs [Poly(NIPAM-hydroxymethacrylate-with disulphide (S-S) linker)/magnetic MWCNTs] | Temperature responsive DOX release | [20] |
| Evans Blue modified carbon nanotube-based | Imaging guided PTT/PDT combined treatment of tumor | [21] |

| | | |
|---|---|---|
| Polymer derived MCNTs [Poly(NIPAM-cyclodextrin-Maleic anhydride copolymer) | Combinatorial Chemotherapy + Photothermal Therapy + Anti-angiogenesis | Present work |

**Table 3.2: Photothermal agents reported in literature for photothermal therapy in cancer management**

| Agents | Materials | References |
|---|---|---|
| Carbon Nanodots | Gd doped, Citric Acid based, Amino acid derived | 22, 23, 24 |
| Gold Nanoparticles | Composite nanomaterials, Polymer modified | 25,26 |
| Graphene Oxide derived materials | Polymer derived | 15, 27 |
| Quantum Dots | Mesoporous silica capped, polymer based, folic acid derived, riboflavin modified, doping with elements (N) | 28,29,27 |

**Table 3.3: Carriers with Chemo/Photothermal Combination therapy/Anti-angiogenesis as a Strategy to achieve antitumor effect**

| Strategy | System | References |
|---|---|---|
| Dual Drug Pair Chemotherapy | Polymeric Vesicles, Micelles, Hydrogels, Mesoporous silica based nanocomposites, Iron oxide nanoparticles based composites, carbon derived materials | 30,31,32 |
| Combinatorial Chemotherapy + Photothermal Therapy | | 33, 34, 35 |
| Anti-angiogenesis | | 36,37,38 |

Certain systems developed for simultaneously aiding chemo and photothermal therapy are concomitant with implications of metastasis and cancer recurrence [13, 14 15, 16.] To overcome these defies, the strategy of administering more than one drug (CCT), was adopted over single drug

therapy [17]. Carbon Nanotubes (CNTs) are strong photothermal converters and have the potential of chemo-thermal combination therapy

They assist intracellular drug delivery and generate heat upon irradiation with NIR (Near Infrared) rays which can promote biological tissue penetration [39],[40]. Further multi-walled carbon nanotubes (MWCNTs) can load much higher cargo of drug and absorb more radiation as compared to single-walled carbon nanotubes (SWCNTs). This property arises due to their nested and cylindrical structures and makes them 20-100 times more efficient than SWCNTs [41]. The use of MWCNTs enriched the carrier's performance to target and combat cancer by the virtue of anti-angiogenesis [42]. This is because angiogenesis associated with tumor plays a very major role in tumor growth and metastasis of cancer due to generation of new vascular growth from the existing ones [43]. Thus the ability to curb development of new blood vessels can aid in the destruction of cancer cells [44]. This opens up a novel approach for targeting the vascular endothelial growth factors, that support angiogenesis at tumor site [45,46]. Antiangiogenic therapy faces limitations of metastasis resulting in tumor invasion which can be overcome by nanotechnology intervened therapy [42]. Surface functionalization of CNTs enhances properties like water dispersion, non-cytotoxicity, cellular uptake and accumulation within tumor. Modification of CNTs with stimuli responsive polymers leads to the design of a smart nanocarrier [10].

Due to a distinctive structure, inherent biocompatibility and amphiphilicity, the oligosaccharide, cyclodextrin (CD) has been used for constructing drug delivery systems by incorporating stimuli response for manifestation of targeted drug release [47, 48, 8.] The amphiphilicity of cyclodextrin (CD) opened up the frontiers for dual drug loading which can be exploited for use in combination chemotherapy. Fabrication of many CD based theranostics is associated with complex synthetic routes like involving various polymerization steps ATRP, RAFT, ROP etc.[49, 50].

The present study was taken up with the aim of addressing issues of conventional cancer therapy via chemo-photothermal combinatorial therapy using a simple and facile strategy. Further previous reports on CNT/CD based drug carriers have demonstrated low drug loading and encapsulation efficiencies which has been improvised in this study [51, 52,53]. The carriers are fabricated to exhibit multidrug delivery with high magnitude of drug encapsulation efficiency

(>90%) and a sustained release over 30 h under tumor microenvironment stimulations and having potential of mild photothermal therapy. To the best of our knowledge, the strategy of chemo-photothermal combination therapy in amalgamation with angiogenesis inhibition has not been reported. The excellent antiangiogenic potential of the carriers loaded with both DOX and Curcumin has been demonstrated ex-ovo by CAM (Chorioallantoic membrane Assay) for the first time. The in-vivo experiments demonstrate that the injectable formulation of these carriers have a profound influence on the decrement of MMP-9 which is associated with tumor progression and metastasis. This shows the potential of the carriers to combat cancer by the synergistic effect of combinatorial CCT-PT and anti-angiogenesis.

## 3.2 Experimental Section

### 3.2.1 Materials

Multiwalled Carbon nanotubes (MWCNTs), β-Cyclodextrin (CD), Maleic Anhydride (MA), Folic acid (FA), Hexamethylene diisocyanate (HMDI), Curcumin, Doxorubicin Hydrochloride (DOX), N-Isopropylacrylamide (NIPAM) and N,N'-Methylene bisacrylamide (MBA) were received from Sigma Aldrich, India and used as such. Fluorescein was procured from Loba chemie. Dimethyl formamide (DMF) was obtained from Spectrochem India, Sulfuric acid and Nitric acid were bought from SD fine chemicals, India. Phosphate buffer saline tablets (for preparation of pH 7.4 buffer solution) were purchased from Sigma Aldrich, India. Glacial acetic acid, Sodium acetate (for preparation of acetate buffer solution) was received from Sisco Research Laboratories (SRL), India.

### 3.2.2 Synthesis of nanocarrier-multifunctional cyclodextrin embedded carbon nanotubes (CD-CNT)

The synthesis of CD-CNT was carried out via various functionalization **(Scheme 3.1)** steps as follows:

**Step 1 Introduction of Carboxyl functionalities on the surface of multi-walled CNTs**: The synthesis was done as per previously reported procedure [54]. Briefly, pristine multi-walled CNTs (1g) were mixed with 250 ml of acid solution having nitric acid and sulfuric acid in 1:3 ratio. The resulting mixture was subjected to ultrasonication for 2 h to obtain a uniform dispersion. The dispersion was then stirred and refluxed at 80 °C for 12 h. After completion of 12 h the mixture

was filtered. The carboxylated CNTs thus obtained were purified by giving washings of methanol and deionized water till the supernatant becomes neutral. The sample was then dried under vacuum at 60 °C overnight.

**Step 2 Preparation of Cyclodextrin-Maleic Anhydride- N-Isopropylacrylamide (CD-MA-NIPAM) polymer:** This polymer was synthesized as per previously reported procedure in chapter 2 [5].

**Step 3 Conjugation of CD-MA-NIPAM polymer and fluorescein with carboxylated CNT via esterification Reaction:** The carboxyl functionalized CNT (50 mg) was dispersed in DMF by sonication for 15-20mins, then CD-MA- NIPAM polymer (65 mg) and Fluorescein (52 mg) were added to the reaction mixture on sonication. (50 mg) of DCC (N, N′-Dicyclohexylcarbodiimide) and (5 mg) DMAP (4-Dimethylaminopyridine) was added and the reaction was kept overnight at room temperature. The reaction mass was vacuum filtered and washed with water followed by washings of acetone. The product obtained was dried.

**Step 4 Conjugation of folic acid via Amide bond formation:** The product obtained from step-3 (100 mg) was dispersed in DMF; folic acid (46 mg) was added and the reaction mixture was sonicated for 15 mins. EDC.HCl (1-ethyl-3-(-3-dimethylaminopropyl) carbodiimide hydrochloride) (50 mg) and NHS (N-Hydroxysuccinimide) (5 mg) were added and the reaction was kept overnight at room temperature. The product was separated by vacuum filtration and washed with water and later with acetone. The product CD-CNT was dried and weighed.

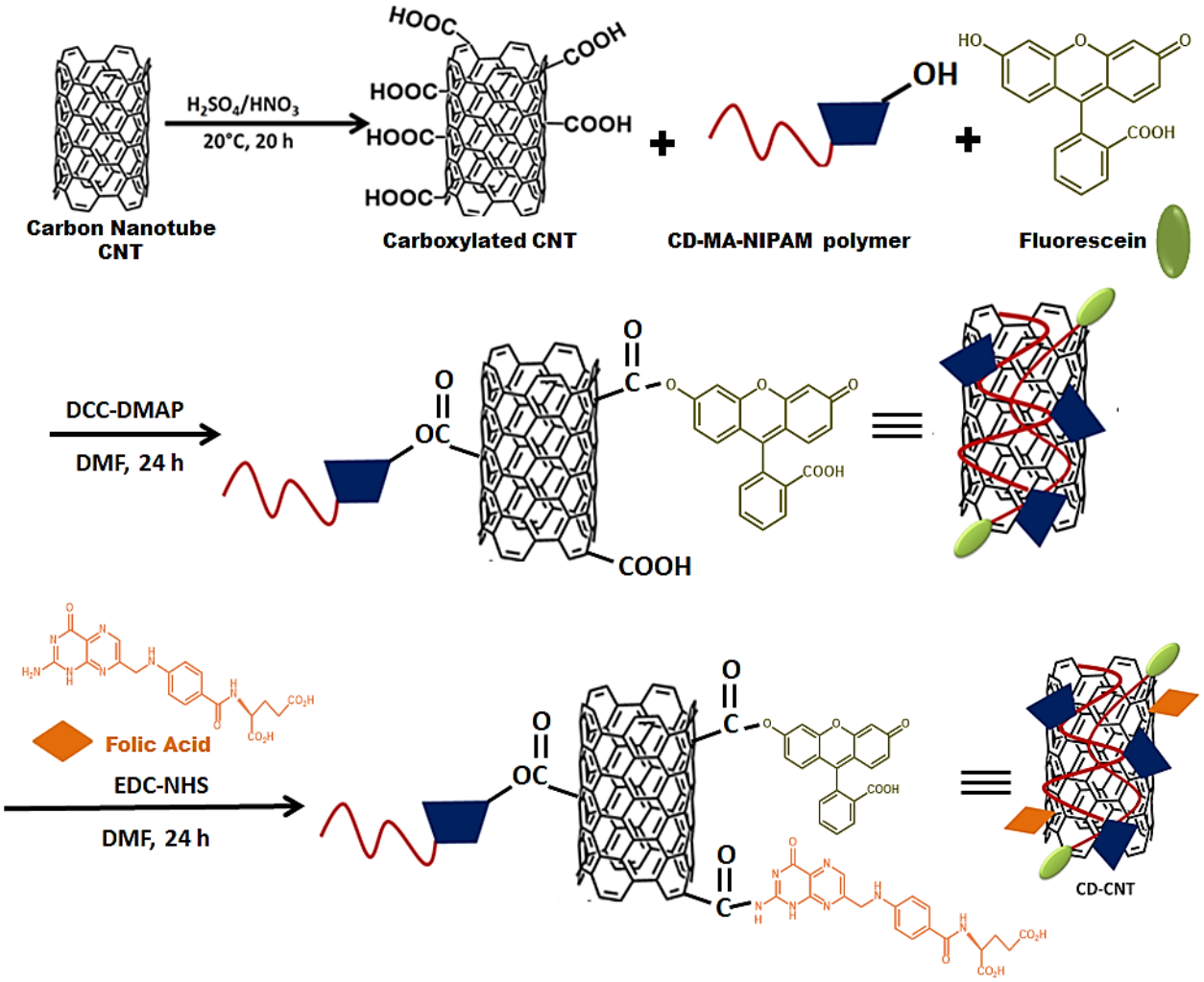


**Scheme 3.1: Synthetic route for CNT embedded Cyclodextrin polymer derived injectable nanocarrier**

### 3.2.3 Characterization

The FTIR spectrum for CD-CNT was recorded using KBr disc method on a Bruker IR Alpha spectrophotometer. The graph was compared with the FTIR spectra of CD-MA polymer and CD-MA-NIPAM polymer reported in chapter 2. The morphology of CD-CNTs was analyzed on a SEM model-JSM-5610 LV, and elemental analysis carried out using a microscope attached to this microscope. A comparison of the morphology and elemental constitution of pristine CNTs with modified ones was made. The fluorescent properties attained due to conjugation of fluorescein with modified CNTs was assessed by UV-vis Spectrophotometric detection on Perkin Elmer Spectrophotometer, Inc, MA, USA and fluorescence studies as recorded on JASCO

FP-6300 spectrofluorometer at room temperature. The confirmation of morphology and size determination of CD-CNT was performed by HR-TEM analysis. The samples were prepared by drop casting method on lacey carbon grids and imaging was carried out on a Joel JEM 2100F model Field Emission Gun microscope at an acceleration voltage of 200 kV. The confirmation of size and thermoresponsive nature of the polymer was made via variable temperature DLS studies on Horiba Scientific Nanopartica SZ-100 in a temperature range of 25-60 °C at a heating rate of 5 °C. Thermal analysis of CD-CNT was performed on TG–DTA 6300 INCARP EXSTAR 6000 in the temperature range of 30–500°C and heating rate of 10 °C/min under inert nitrogen atmosphere. The photothermal efficiency of modified CNT was ascertained using both CD-CNT and drug loaded CD-CNT. An 808 nm NIR laser source having 1.0 W power was used for the experiments and the temperature changes were recorded on TP101 sensitive thermometer. An effect of photothermal therapy on drug release and cell viability was assessed. For the in-vitro cellular imaging a Floyid cell imaging station (Life Technologies, USA) at 400X resolution was employed. The internalization of CD-CNT and cell viability of drug loaded CD-CNT was observed and photographed.

### 3.2.4 Determination of Photothermal Efficiency of CD-CNT

The dispersed solutions of CD-CNT (2.5 mL, 25 $\mu g \cdot mL^{-1}$) was placed in a quartz cell (12.5 × 12.5 × 45 mm3 ) and exposed to a continuous wave emerging from an 808 nm NIR laser diode having an output power of 1.0 W [24]. The temperature of the solution was measured every 30 s using a TP101 sensitive thermometer.

### 3.2.5 Preparation of Drug loaded CD-CNT

The loading of drug on CD-CNTs was carried out via batch technique by maintaining the ratio of drug versus polymer as 1:1 [5,25]**.** Curcumin and DOX.HCl were loaded simultaneously by taking them in 60:40 ratios. Accordingly drug solution of 30 mg/mL concentration was made by dissolution of 90 mg curcumin and 60 mg of DOX.HCl (total quantity of drug-150 mg) in 5 mL of 1:1 solution of water and ethanol. For drug loading on CD-CNT, 150 mg of sample was dispersed in a vial with 30 mg/ml of 5 mL and stirred overnight in dark. Post encapsulation ,the drug loaded carriers were obtained from drug solution via centrifugation. For removal of free drug, the separated drug carriers were given washings of ethanol twice. The drug-loaded CD-

CNT then dried at room temperature overnight and later preserved in desiccators. Calibration plot was constructed on UV- spectrophotometer for curcumin at 430nm and for DOX at 480 nm to quantify the concentration of drug in supernatant. The drug entrapment efficiency (%LE) and drug loading content of nanocarrier was estimated by using following equations [55, 52] .

$$\%\ enrapment\ efficiency = \frac{Ic-Sc}{Ic} \times 100 \quad \text{---------- (1)}$$

Where $I_C$ denotes initial content of curcumin added and $S_C$ represents curcumin concentration in supernatant.

$$\%\ drug\ loading\ content = \frac{Weight\ of\ drug\ in\ nanocarrier}{Weight\ of\ drug\ loaded\ nanoparticles} \times 100 \quad \text{---------- (2)}$$

### 3.2.6 Drug Release Experiments for CD-CNT

The release experiments were performed in an Erlenmeyer flask in PBS buffer (0.1 M, pH 7.4) and in Acetate Buffer (pH- 5.0) for drug loaded CD-CNT at two different temperatures 37°C and 40°C. We next investigated the release behavior of curcumin and DOX by varying physiological conditions of pH and temperature in order to mimic cellular environments. 10 mg of drug loaded CD-CNT were suspended in 25 mL of release medium and kept under constant stirring maintained at 37 °C. 3 mL of samples were periodically removed and content of drug released was determined using UV-vis spectrophotometer. The volume of each sample withdrawn was replenished by the same volume of fresh release medium. To assess the effect of drug release by PT conditions, the release profiles were monitored in the presence and absence of laser irradiation. All the release studies were performed in triplicate and mean values have been plotted in the cumulative drug release profiles. The release media was exposed to a continuous wave emerging from an 808 nm NIR laser diode having an output power of 1.0 W for 30 s at 0 min and drug release was assessed at different time intervals [24].

### 3.2.7 IN-VITRO STUDIES

The in-vitro studies were performed as per the protocols mentioned in chapter 2. Briefly the following parameters were assessed cell viability assay via MTT (on two different cell lines Hela (Human Cervical Cancer Cell line) and MCF-7 (Human Breast Cancer Adenocarcinoma Cell

Line), Hemolysis assay, internalization test and assessment of cell mortality by PI staining technique.

### 3.2.8 Ex-ovo studies for assessment of antiangiogenic potential of the drug loaded CD-CNT

#### 3.2.8.1 Chick Chorioallantoic Membrane (CAM) Assay

Shell-less culture of chicken embryo is an experimental model system that undergoes vascular network development that can be studied and photographed from 4 h to 120 h post-hatch. Parameters such as blood vessel network, vessel density, segments and branching points in CAM are indicators of normal angiogenesis and, any changes in the same suggest possible anti-angiogenic potential of the test compound [56].

The experimental protocol (MSU-Z/IAEC/03-2017) was approved by the Institutional Animal Ethical Committee (IAEC) and the Committee for the Purpose of Control and Supervision of Experiments on Animals (827/GO/Re/S/04/CPCSEA). The procured eggs were incubated under standard conditions (37.5 °C, humidity 60%) for 60 hours and guidelines of Committee for the Purpose of Control and Supervision of Experiments on Animals (CPCSEA) were hereby followed for all the experiments conducted on the chicken embryo. Later eggs were explanted into shell-less culture as per reported procedure[57]. The Shell less embryos were incubated for another 48 h in Thermoscientific MIDI 40 $CO_2$ incubator. Dosing was done directly on a network of blood vessels using a micropipette and embryos were incubated for 4 h.

#### 3.2.8.2 Quantitative real-time polymerase chain reaction (qPCR) analysis

Total RNA was isolated from vessels of control and treated embryo using Trizol reagent and cDNA was synthesized using iScript cDNA Synthesis kit (BIO-RAD CA, USA). m-RNA levels of candidate genes (FGF2 and VEGF) were quantified by qPCR analysis (Quant-Studio-3 real time PCR, Life Technologies, CA, USA) using SYBR Select Master Mix. The list of primers used for real time PCR is shown in **table 3.4.** The data were normalized to the internal control GAPDH and analyzed using 2-ΔΔCT method.

**Table 3.4: List of primers for Real time PCR**

| | |
|---|---|
| GAPDH | Forward: GTGGTGCTAAGCGTGTTATCATC |
| | Reverse: GGCAGCACCTCTGCCATC |
| FGF2 | Forward: GGCATGAAATGTGCAACAG |
| | Reverse: TCCAGGTCCAGTTTTTGGTC |
| VEGF | Forward: TGAGGGCCTAGAATGTGTCC |
| | Reverse: TCTTTTGACCCTTCCCCTTT |

### 3.2.9 *In-vivo* studies for anticancer potential

The procurement of Laboratory animals (Balbc mice 28-30 g n= 24, male/female) was done from Zydus Research Center, Ahmedabad, India. Animals were housed under LD 12:12 with food and water ad libitium as per the standard conditions. Institutional Animal Committee (IAEC) and CPCSEA granted the ethical clearance for animal experimentation. The animals were classified as Experimental groups (n=6 per group) viz untreated equal to control, intraperitoneally injected with HEPG2 cells. The animals were treated so as to develop hepatic tumor (HCC), the comparison of treatment was observed based on HCC animals treated with 2.5 mg/ml, 110 µL of Doxorubicin (DOX), and HCC animals treated with nanocarriers loaded with DOX. The nanocarriers and drug loaded nanocarriers were dosed as injectable formulations intraperitoneally. The experiment was continued for 15 days. After completion of 15 days body weights were recorded, 0.8 mL of blood was collected by retro-orbital sinus puncture and serum was separated in cold centrifuge (3000 rpm). Standard kits used for analysis of various parameters are as per the mentioned in chapter 2.

### 3.2.10 Statistical analysis

All experiments have been performed at least in triplicate and expressed as means ± standard deviation (SD). The differences among groups were analyzed using the paired, two-sided Student's t-test. P-value < 0.05 were considered significant, and P-value < 0.01 were considered to be highly significant.

### 3.3. Results and discussion

#### 3.3.1 Rational design of CD-CNT and its characterization

The multi-hydroxyl groups of CD were utilized to synthesize dual stimuli responsive crosslinked polymer which was covalently attached to CNTs to engineer smart nanotheranostics. The first problem which needs to be addressed for preparation of CNT based nanocarriers for drug delivery is to reduce their cytotoxicity and make them biocompatible. Purification of the CNTs by mixed acid treatment helps to get rid of the impurities and makes them suitable for biological use [58]. In addition, the surface of CNTs gets decorated by carboxyl functionalities which improvises their dispersity and makes them suitable for further desired chemical modification [51]. In this work we have introduced further modifications on the surface of CNTs by attachment of a stimuli responsive CD polymer which can respond to pH and temperature variations in the external environment. The carriers are further supported by folic acid expecting targeted delivery and by fluorescein to monitor the movement of the carriers. The NMR of the CDMA co-polymer has been previously reported [59]. The successful assortment of all the required functionalities was confirmed by the presence of relevant functional groups in the IR spectra. The FTIR spectrum **(figure 3.1A)** of CD-CNT confirmed the presence of the characteristic bands corresponding to the CDMA-NIPAM polymer and the characteristic peaks of MWCNTs at 1616 $cm^{-1}$ [60]. Shifts are observed in the bands which are due to the interaction of the functionalities with the CNTs. The bands at 2853 $cm^{-1}$ and 2929 $cm^{-1}$ corresponds to N-H stretching frequencies [61]. The peaks at 1125 $cm^{-1}$ showing C-O stretching frequency and 768.75 $cm^{-1}$ that appears due to C-H bending frequency [62]. The -CH2 scissoring vibration peak was observed at 1457 $cm^{-1}$, -$CH_3$ bending vibration appears at 1385 $cm^{-1}$, peak at 1366 $cm^{-1}$ shows C-H bending vibration, and that at 1169 $cm^{-1}$ appears due to bending vibration [62], [63].

It is observed from the SEM micrographs demonstrated presence of tubular objects that confirms the presence of CNTs **(figure 1B).** It was further observed that dispersion of modified CNTs is better as compared to that of bare CNTs. The elemental composition indicated presence of only elemental carbon in pristine CNTs. Successful conjugation is indicated by the presence of C, N and O in the graph of CD-CNT in addition to the presence of C **(figure 3.1B).**

The UV-visible spectra and fluorescence spectra analysis **(figure 3.1C & 3.1D)** demonstrated a broad absorbance band ranging from 490 to 580 nm with emission maxima at 516 nm corresponding to fluorescein thus confirming its conjugation. The fluorescent carriers as

observed under UV light are shown in **figure 3.1C**. The inherent fluorescence of the carriers makes them applicable for non-invasive luminescence imaging. Such fluorescence imaging aids in the tracking of drug release *in-vivo* and provides information about tumor progression and regression in the animals [64]

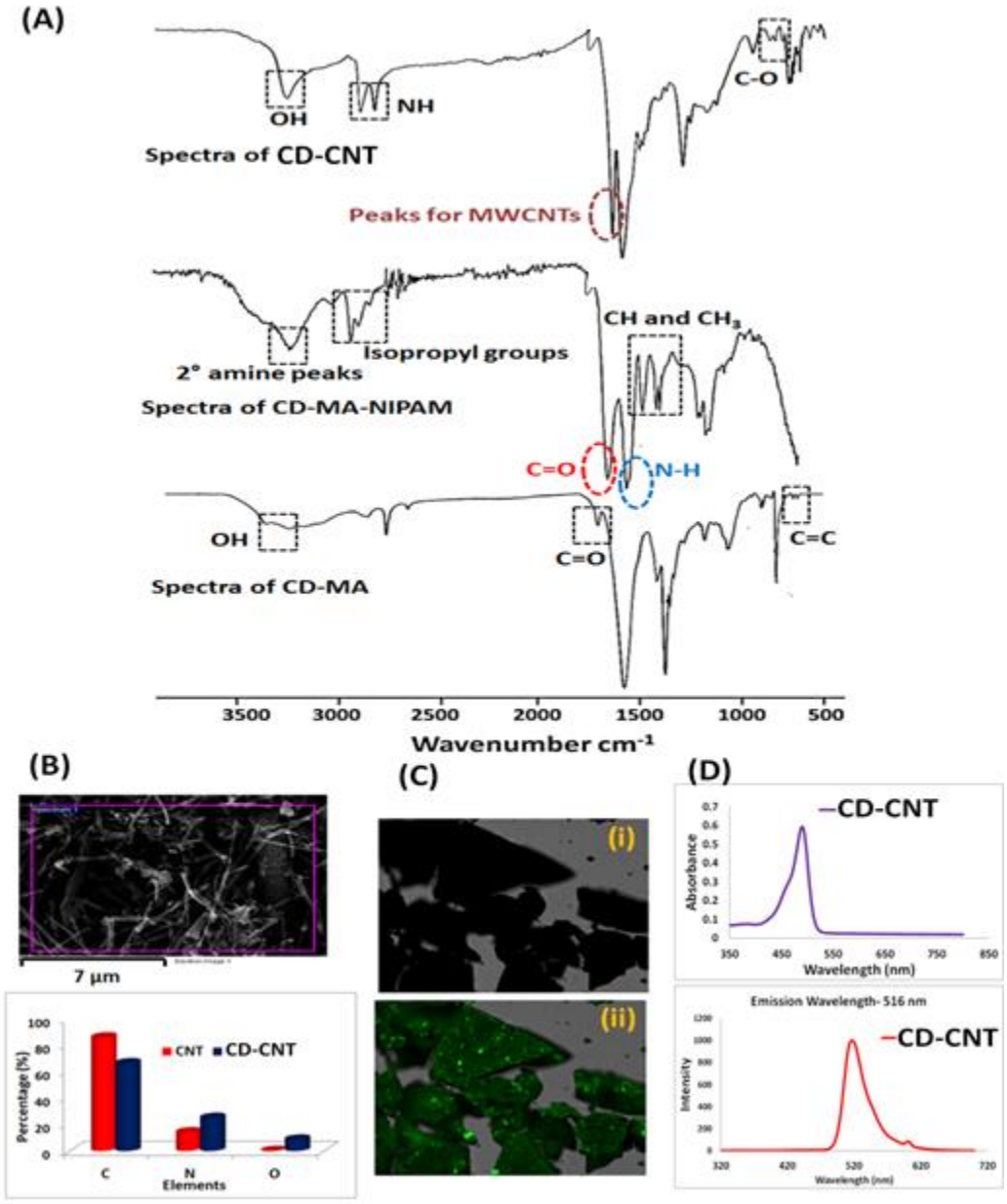


**Figure 3.1: (A) IR spectra of CD-MA polymer, CD-MA-NIPAM polymer and nanocarrier CD-CNT (B) SEM image of CD-CNT and difference in elemental composition of nascent CNT and CD-CNT (C) Fluorescent Images of (i) nascent CNTs and (ii) CD-CNTs (D) : UV-vis and PL spectra of CD-CNT**

The temperature responsiveness of the carriers was assessed using variable temperature DLS experiments and demonstrated in **figure 3.2A**. It was observed that the size of the particles varied with the change in temperature [65]. At 25°C, the hydrodynamic diameter was 374 nm. A sharp transition was observed at 40°C, where the size reduces to 258 nm. Thus 40°C is the transition temperature for the thermoresponsive polymer. The diameter of the particles decreases due to the dehydration of polymer chains and collapse of the hydrophilic segments of PNIPAM (Poly N-Isopropylcrylamide) above the transition temperature.

The strategy of combining photothermal therapy with chemotherapy provides a platform of mitigating multidrug resistance via non-conventional approaches. As per reports, it takes more than 10 days to achieve a tumor inhibition rate in a range of 60-95% [66]. On the other hand an administration of photothermal therapy at higher temperatures (greater than 50 °C) can cause serious side effects like skin damage in addition to tumor cell destruction. This is a hindrance for the clinical use of PT based treatments. Thus an approach is needed which aid in the use of PTT synergistically with other treatment which can cause minimal damage to normal cells and damage tumors selectively. In this purview the optical response of the modified CNTs on exposure to the irradiation was assessed. It was observed that on exposure to Laser for 5 minutes the temperature of the solution in the cuvette reaches 52 °C **(figure 3.2B)**.

This suggests that an exposure to laser less than 5 minutes is sufficient to create a photothermal effect. The heating effect created due to photothermal therapy induces an oxidative stress [67] on the cancer cells which leads to apoptosis. Thus the synthesized nanocarriers can be used for combinatorial therapy as they can cause a targeted dual drug release to affect the multi-drug resistance and they can be used for mild PTT (temperature- 45-50 °C) to enhance cancer cell damage without the induction of heavy skin damage. Thus the modified CNTs are efficient vectors for overcoming the challenges in conventional cancer therapy [17].

The TGA curves in **figure 3.2C** show the carriers are thermally stable upto temperatures as high 500 °C. A three stage thermal degradation was observed as per previous reports [5].

The nanosized was confirmed from HR-TEM as shown in **figure 3.3;** the micrographs suggested that the diameter of nascent CNTs was 200 nm. An increase in the diameter of CNTs is observed upon functionalization. The average diameter of CD-CNTs was observed to be 370 nm. A decrease in the contrast in the images corresponds to the formation of a polymeric shell over the

surface of CNTs **(figure 3.3E)**. Upon successful drug loading the darker contrast is retained **(figure 3.3F)** [68].

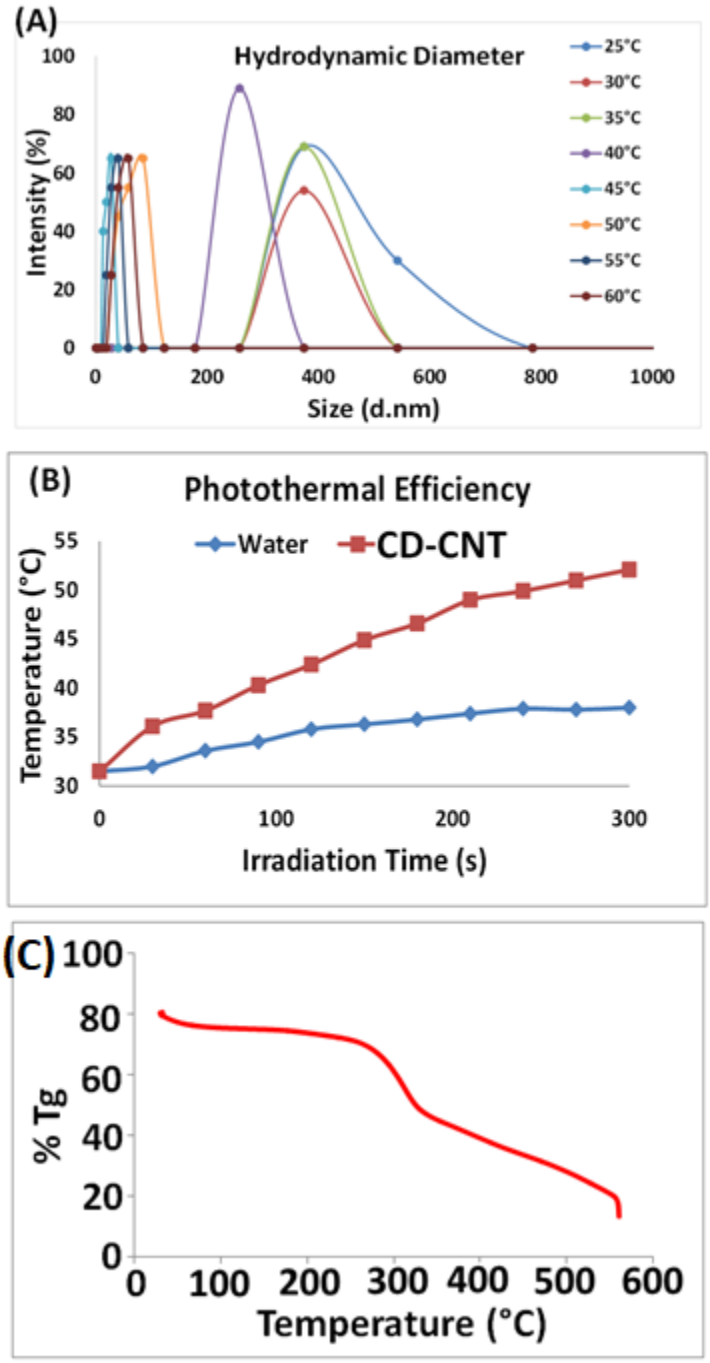


**Figure 3.2: (A) DLS spectrum and (B) heating performance upon irradiation with laser and (C) TGA curve of CD-CNT**

These analytical characterizations suggest formation of the multifunctional carbon nanotubes as with successful attachment of desired functionalities. The carriers were then explored for their drug loading and release potential.

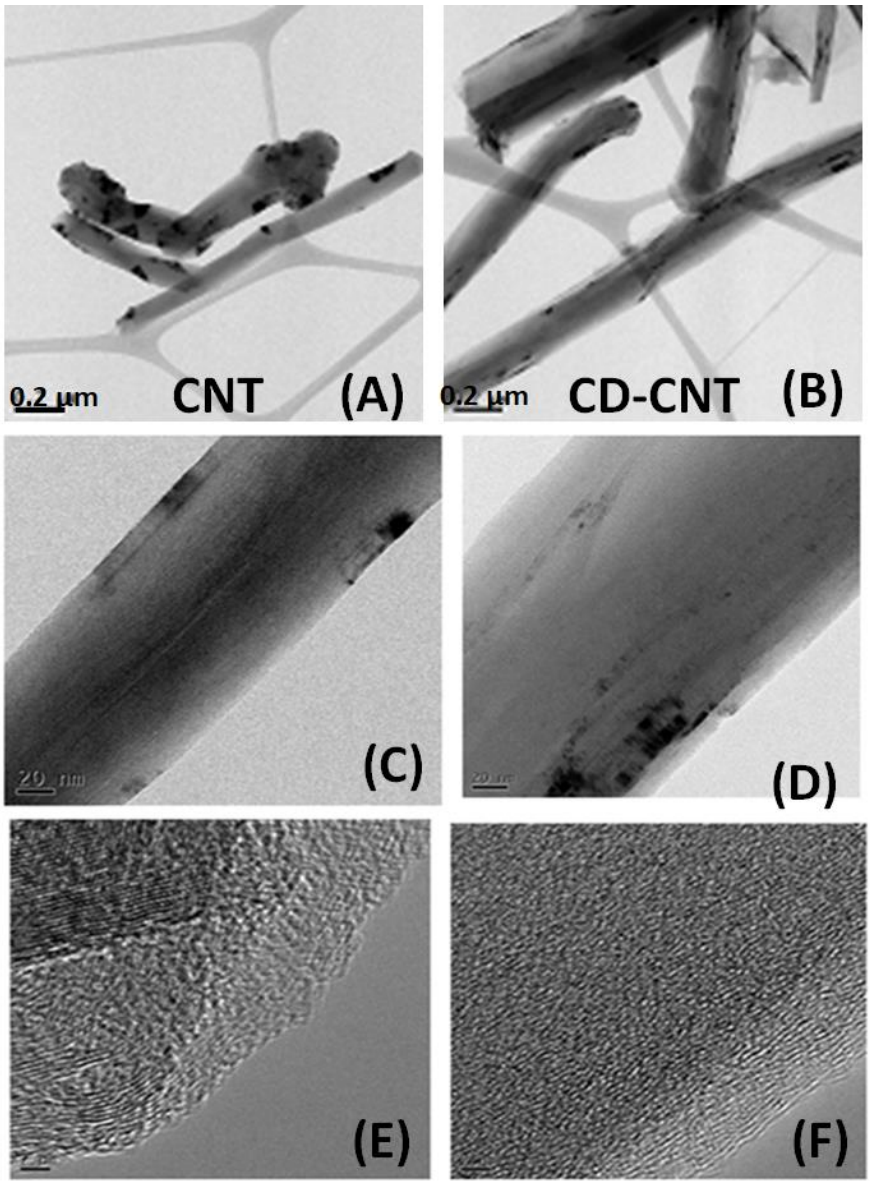


**Figure 3.3: TEM images of (A) nascent CNT and (B) nanocarrier; High Resolution TEM images at 20 nm magnifications of (C) nascent CNTs and (D) nanocarrier and at 5 nm magnification of (E) nanocarrier and (F) Drug loaded nanocarrier**

### 3.3.2 *In-vitro* drug loading and release

An enhanced drug entrapment efficiency of 92 % was observed. The drug loading content of 28.8 wt% for curcumin and 19.09 wt% for DOX were observed. **Table 3.5** shows a comparison of drug loading and capabilities of various reported carriers.

**Table 3. 5: Comparison of drug entrapment and loading efficiencies for various carriers**

| Sr. No. | Drug Carrier | Drug Entrapment Efficiency (%) | Drug Loading Efficiency (%) | Reference |
|---|---|---|---|---|
| 1 | PEG-PAA Nanogels | 92 | 18 (DOX)<br>18 (CDDP) | [69] |
| 2 | B-CD-NIPAM | 83 | 1 (PTX) | [53] |
| 3 | Carboxyl functionalized MWCNTs | 19.7 | 9.8 (Ru polypyridyl complex) | [18] |
| 4 | Mesoporous silica based polymer ($SiO_2$-PMAA-b-PNIPAM) | 90 | 21 (DOX) | [52] |
| 5 | CD-CNT | 92 | 28.8 (curcumin)<br>19.09 (DOX.HCl) | This work |

The increased drug loading was observed because of use of CNTs as the platform material for attachment of functionalities. The drug molecules have a capacity to be entrapped within the cylindrical structures of CNTs via π-π stacking interactions [70],[18] in addition to their interactions with cyclodextrin moieties and stimuli responsive carrier. The cumulative release curve of curcumin as shown in **figure 4.1A** shows a lower release rate mostly below 20 % at physiological temperature and acidic pH. On the contrary at elevated temperature and pH 7.4 cause a release greater than 85% was obtained. On the other hand it was observed that DOX release **(figure 4.1B)** (was less than 30% under pH 7.4 whereas under acidic conditions a cumulative release of 70 % was observed which is further enhanced to 90% at higher temperature (40°C).

The observations are in agreement with the previous finding reported by our group [5]. The difference in the release profile of curcumin and DOX.HCl is a result of difference in chemical structure of both the drugs and their interaction with the carrier. DOX.HCl bears positively charged protons on its structure at pH 7.4, which interacts with the negatively charged $COO^-$ groups on the polymer chains via electrostatic forces of attraction. These interactions cause drug molecules to adhere onto the carriers resulting in its slow diffusion into the media. Conversely, when the media is acidic (pH 5), the carboxylate ions undergo protonation causing the polymer to shrink and disturbing the electrostatic interactions between polymer and drug that facilitates an enhanced drug release [71].

Curcumin being hydrophobic has an ability to encapsulate in the hydrophobic cavity of CD, in addition to its entrapment in the polymeric matrix [5]. Thus CD molecules play a crucial role in elevating the drug payload of hydrophobic drugs. Apolar-apolar association upon entrapment of curcumin causes the ring strain of CD molecules to decrease thus causing facilitated entry of curcumin over water molecules (Loftsson & Brewster, 1996). The curcumin release profile shows an opposite trend as compared to DOX release. This is due to the fact that electrostatic interactions cannot exist between curcumin and polymer due to its structure.

Increasing the temperature of release media causes an increase in the release of both DOX and curcumin which is attributed to the presence of thermoresponsive CD-MA-NIPAM co-polymer. The enhanced release of drug at elevated temperatures is because of conformational coil to globule transformation in the polymer at the transition temperature (Lower critical solution temperature LCST-40 °C). At temperatures below LCST the polymer forms hydrogen bond with surrounding water molecules causing hydration (Shiraga, Naito, Suzuki, Kondo, & Ogawa, 2015). Above LCST, the water molecules are dispensed out of the polymer matrix resulting in a partial degradation and agglomeration of the polymer chains and a rapid diffusion of entrapped drug molecules in the media.

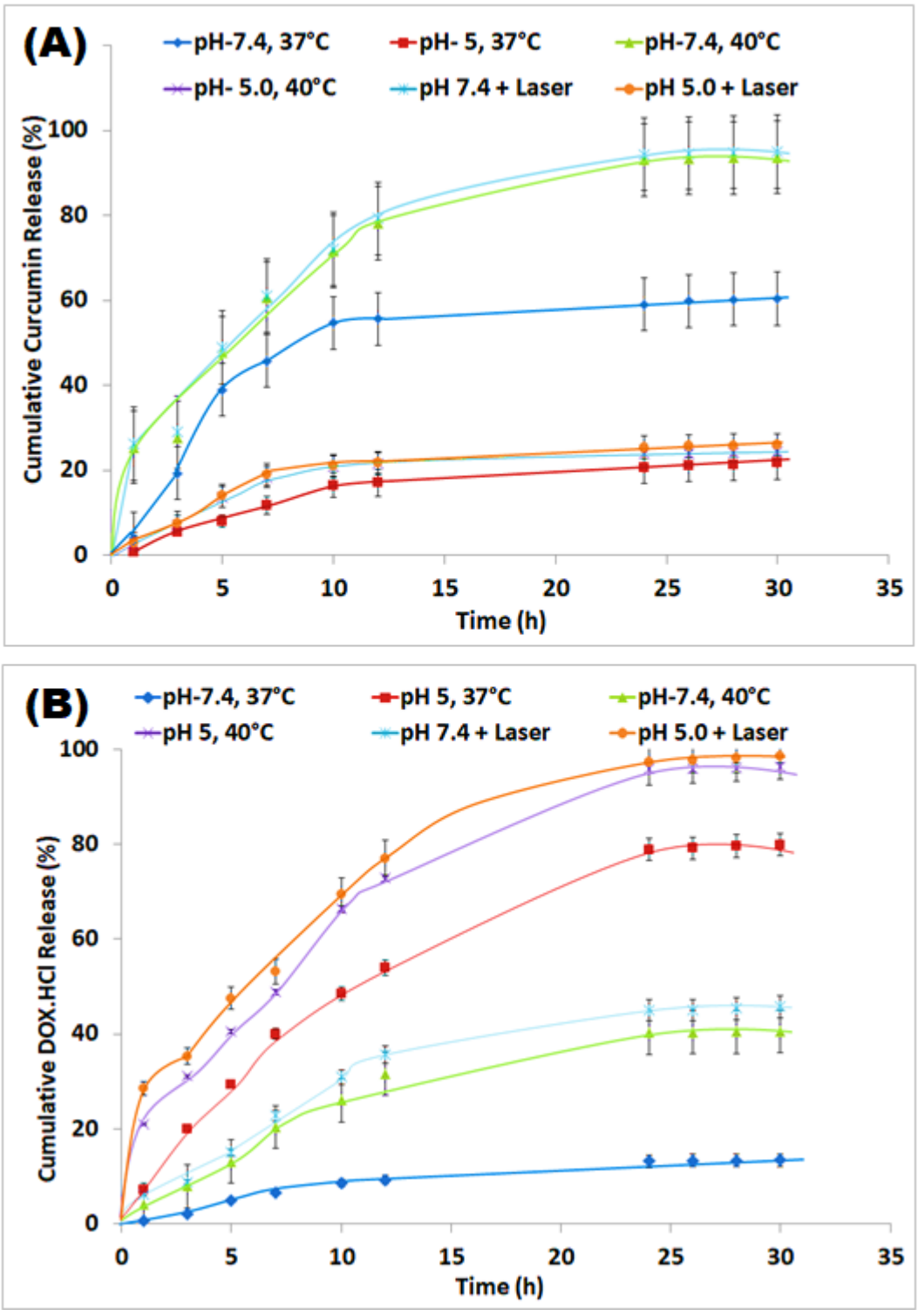


**Figure 4.1 Release profiles of (A) Curcumin and (B) DOX.HCl from nanocarrier under dynamic conditions of pH, temperature and photothermal trigger using NIR laser of 808 nm.**

An enhanced drug release was observed for both the drugs under the influence of photothermal conditions. Thus the carriers are able to target release in typical micro-environments of intracellular lysosomes or endosomes or cancerous tissue, which would be beneficial for elevating the drug bioavailability and avoiding the systemic toxicity of DOX **(figure 3.5)**.

The capability of inducing photothermal effect helps to achieve the anticipated therapeutic effect with reduced amount of drug. This helps to abate the potential toxic effects that can arise due to either drug or CNTs. The presence of a stimuli responsive polymer attached to the CNTs aids in maximum drug release under the conditions of tumor microenvironment. This helps in drug retention and any potential loss of drug before the target site is reached thus enhancing the therapeutic efficacy of the drugs. On exposure to NIR irradiation the drug release from the carriers is enhanced thus showing a better possibility of tumor regression[34].

It was observed that upon irradiation with NIR the DOX release does not exhibit a substantial increase. After 30 h the release of DOX.HCl at higher temperature is 96% in the presence of laser the release is 98% thus suggesting a comparable drug release upon laser exposure. Similar phenomenon is observed in case of Curcumin release from CD-CNT; at higher temperature 94% curcumin is released whereas upon laser irradiation 95% of release is observed. This suggests that NIR irradiation does not perturb the sustained release behavior of the drug carriers. Thus, the release of the drug is not disturbed and CD-CNTs are potential materials which can help for achieving a chemo-thermal combinatorial therapy.

### 3.3.3 *In-Vitro* Studies

#### 3.3.3.1 Assessment of *in-vitro* cyto-compatibility and hemocompatibility of carriers

The non-toxicity of the carriers was estimated by MTT assay on Hela and MCF-7 cell lines as shown in **figure 3.6 and 3.7**. The carriers (CD-CNT) showed a cell viability of more than 80 % cell viability indicating that the carriers are nontoxic. These experimental findings support the literature reports that; cytotoxicity of CNTs and the subsequent non-biocompatibility can be drastically reduced by surface modification [70]. Thus the synthesized carrier is suitable as drug delivery vehicle. A decrease in cell viability upon irradiation with NIR laser is attributed to the photothermal efficiency of carriers by virtue of CNTs [17]. The hemolysis assay performed on erythrocytes revealed that carriers do not show any decremented effect on the survival of RBCs

**(figure 3.8A)** and thus suggest their hemocompatibility. This confirms the application of the nanocarriers for injectable formulations.

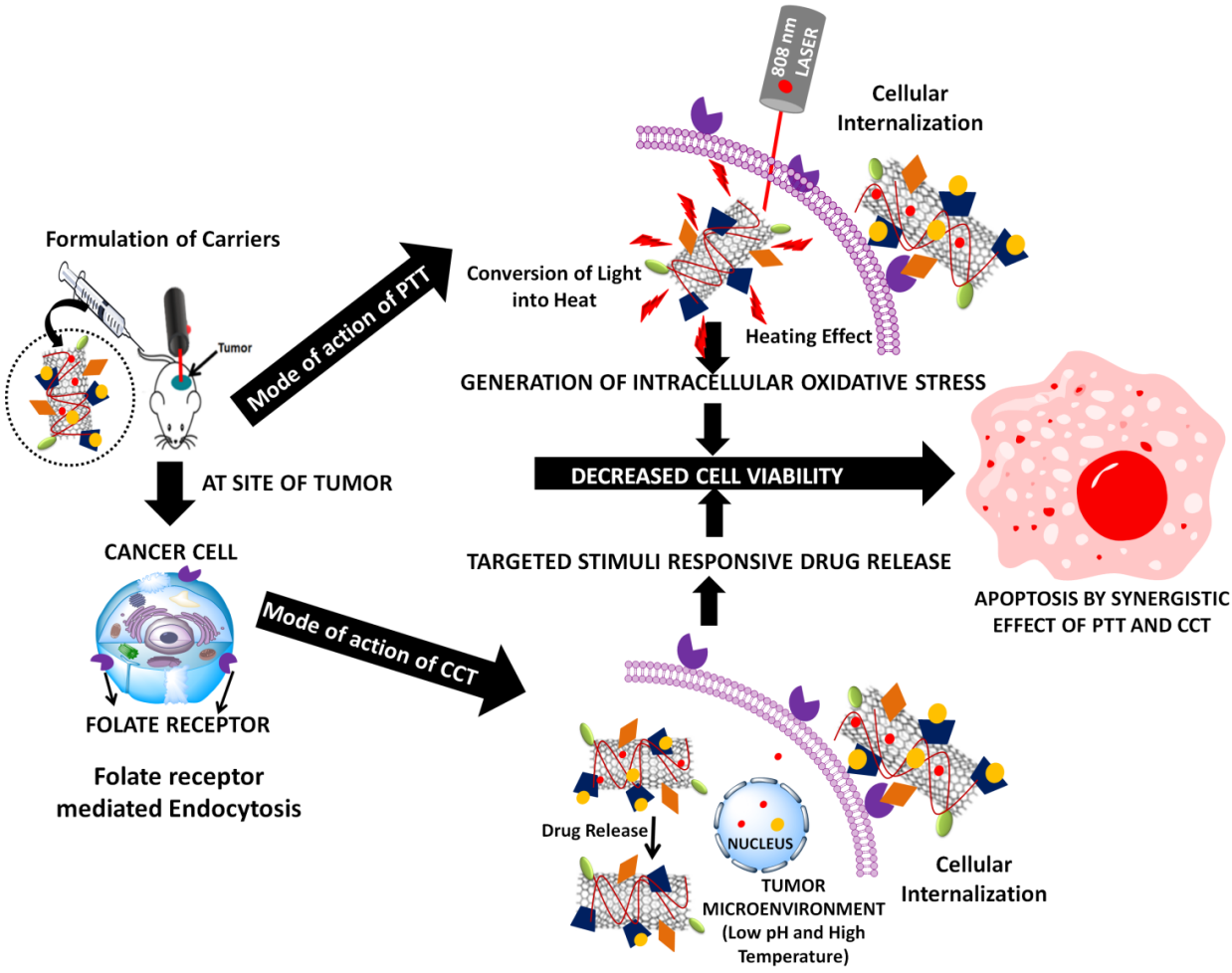


**Figure 3.5: Mode of action of the carbon nanotubes based drug carriers for combating cancer via stimuli responsive dual drug delivery synergistically with photothermal therapy**

### 3.3.3.2 Assessment of internalization of the carriers

The nanocarriers are inherently fluorescent and can auto-fluoresce under green filter (Ex/Em: 485-520 nm). The results of internalization as depicted in **figure 3.8B** exhibit prominent fluorescence within the cell post- treatment with CD-CNT. This confirms the capability of nanocarrier to cross plasma membrane and get internalized in the cytosol of the cells which is imperative for drug delivery devices for a targeted delivery. Healthy cellular morphology was observed which confirms the findings of cell viability assay.

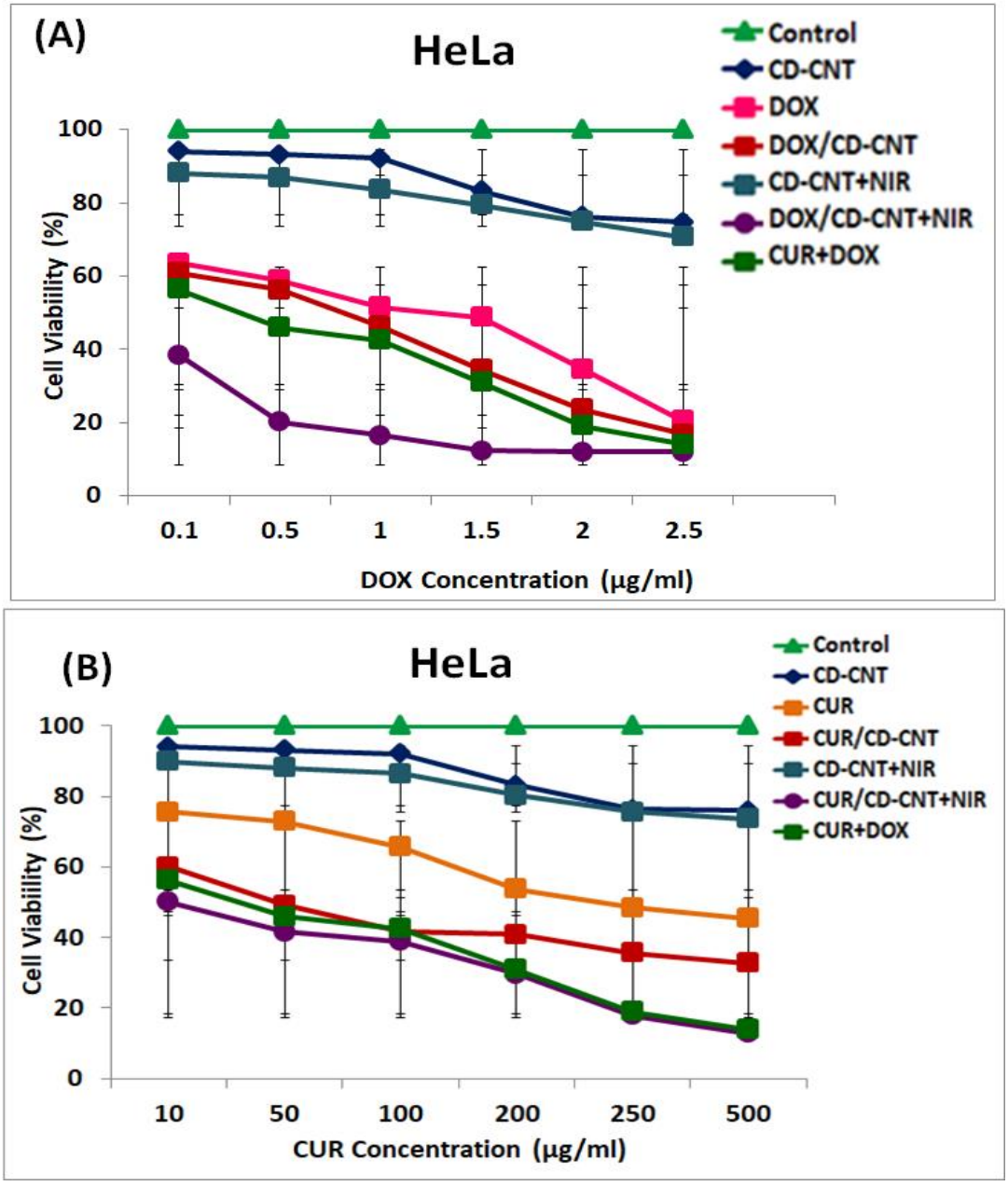


**Figure 3.6: Cytotoxicity studies of HeLa cell lines incubated with curcumin, nanocarrier and curcumin loaded nanocarrier for 24 h with and without NIR irradiations. All cell viabilities were tested in three replicates (n = 3) the results are expressed as Mean ± SD**

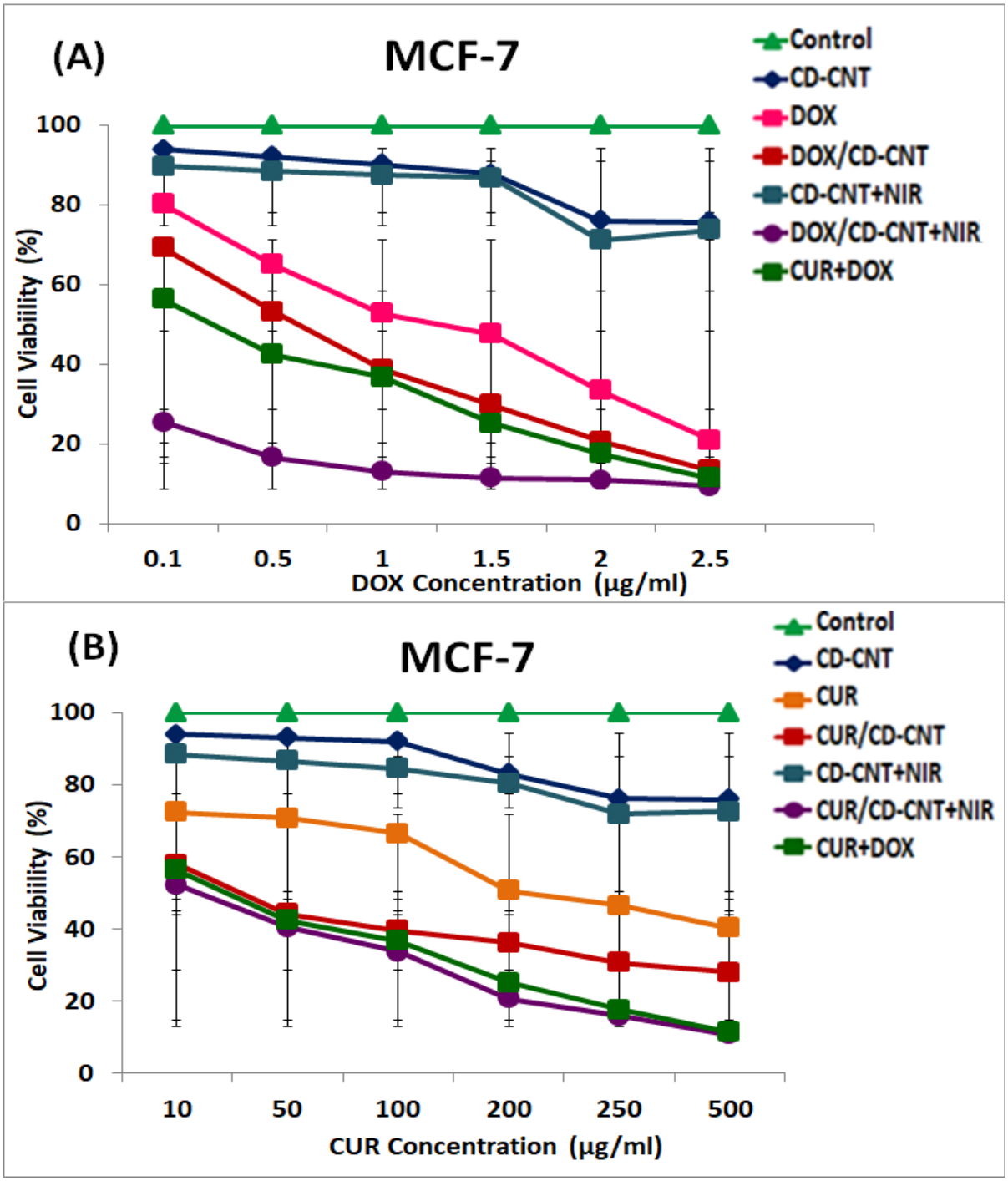


**Figure 3.7: Cytotoxicity studies of MCF-7 cell lines incubated with Dox, nanocarrier and Dox loaded nanocarrier for 24 h with and without NIR irradiation. All cell viabilities were tested in three replicates (n = 3) the results are expressed as Mean ± SD.**

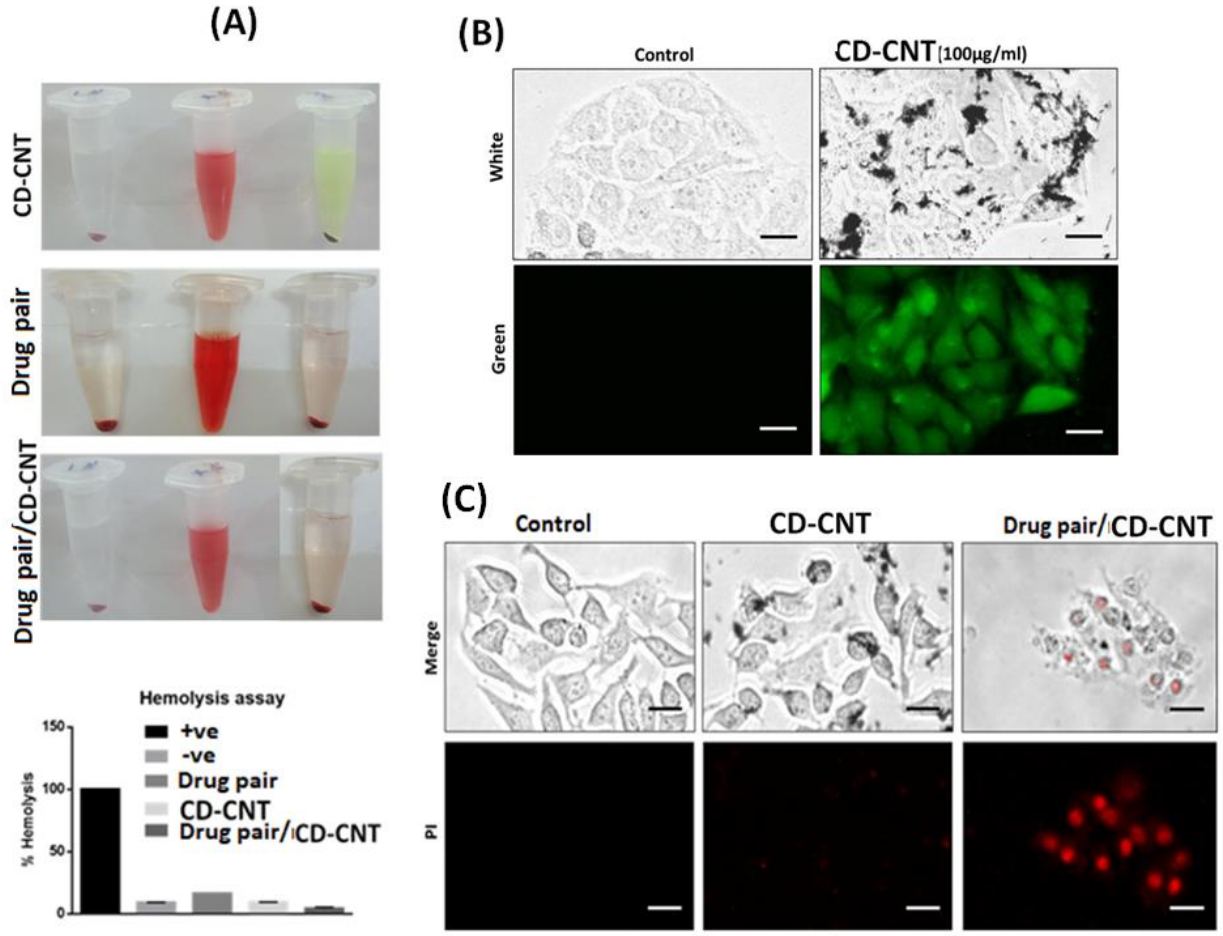


**Figure 3.8: Hemolysis assay of Drug pair, CD-CNT and Drug pair loaded CD-CNT. (B) Internalization of nanocarrier in HeLa cell line and (B) PI staining of Hela cells. Cells undergoing apoptosis were stained by PI (At Scale bar-20µm)**

### 3.3.3.3 Assessment of in-vitro cytotoxicity of drug loaded carriers and the effect of photothermal therapy on apoptosis

The drug loaded nanocarrier causes a significant decrement in the cell viability. The decrease in cell viability is much more as pronounced as compared to the treatment with only drugs suggesting improvement in antitumor efficacy of the drugs upon being dosed using the carriers. It was observed that the cell death is more pronounced in the MCF-7 cell lines as compared to that in HeLa cell lines. This can be attributed to the presence of overexpressed folate receptor mediated enhanced invasion of the folic acid decorated carriers towards MCF-7 cells [72]. Further it was observed in figure 6&7 that the combination of chemotherapy and photothermal therapy

(labeled as CUR/CD-CNT+NIR or DOX/CD-CNT+NIR in the graphs) was much more efficacious when the therapies were individually applied (labeled as CUR/CD-CNT or DOX/CD-CNT in the graphs for chemotherapy and CD-CNT+NIR for photothermal therapy). The cell death increased by almost 10% and 40% in case of chemo-photothermal combinatorial therapy as compared to chemotherapy and PTT individually on both the cell lines.

**Combination Index Analysis:**

The performance of the selected drug pair (CUR and DOX) towards induction of cocktail chemotherapy was evaluated by cytotoxicity studies on 2 different cell lines (MCF-7 and HeLa). This was established by calculating the combination index (CI) of the drug pair which quantitatively measures the combination effect [17,69]. The CI was calculated as per the following equation:

$$\mathbf{CI}_{CCT} = \left[\frac{IC_{50}(Combination\ DOX)}{IC_{50}(DOX)}\right] + \left[\frac{IC_{50}(Combination\ CUR)}{IC_{50}(CUR)}\right] \quad \text{-------- (4)}$$

Here,

$CI_{CCT}$ depicts the combination index of cocktail chemotherapy, $IC_{50}$ (combination DOX) and $IC_{50}$ (combination CUR) represents the half inhibitory concentration of DOX and CUR used in combination. $IC_{50}$ (DOX) and $IC_{50}$ (CUR) shows the half inhibitory concentration of the single drug used to attain the equivalent effect. When CI <1, CI=1 and CI>1 the system exhibits a synergism, combination and antagonism behaviour respectively.

The smaller CI value observed in case of MCF-7 cell lines suggest the drug pair shows superlative cocktail effect thus an enhanced antitumor efficiency on breast cancer as compared to HeLa cells as a result of folate receptor induced specificity. The values of CI obtained for the therapy induced by our synthesized nanocarriers **(Table 3.6)** are less than 1 on both the types of carcinoma suggesting a synergistic effect of the drugs in chemotherapy.

**Table 3.6: Combination Index for DOX-CUR paired dual drug treatment using CD-CNT.**

| Entry | $IC_{50}$ (DOX) (µg/ml) | $IC_{50}$ (CUR) (µg/ml) | $IC_{50}$ (Combination DOX+CUR) (µg/ml) | $CI_{CCT}$ |
|---|---|---|---|---|
| **HeLa** | 3.05 | 5.02 | 1.75 | **0.91** |
| **MCF-7** | 3.50 | 4.61 | 3.5 | **0.71** |

The assessment of cell viability upon the NIR irradiation in those cells dosed with drug loaded nanocarriers shows interesting data. It was observed from (**figure 6 & 7)** that the cell mortality rate was almost more that 80% when the cells are given NIR irradiation. This indicates that photothermal effect enhances the cellular internalization of the carriers which promotes drug to easily enter the cytoplasm and nucleus producing an enhanced cell death.

### 3.3.3.4 Assessment of cell mortality

The cell mortality was assessed via propidium iodide (PI) staining experiments **(figure 8C)**. The Drug loaded CD-CNTs showed accounted for more cell death which is observed in the form of more cells showing PI positive staining. These results provide positive qualitative evidence on nanocarrier mediated increased uptake of drugs that accounts for visibly higher cell mortality.

### 3.3.4 Assessment of ex-ovo anti-angiogenesis potential of the nanocarriers

As the CCT demonstrated synergistic effect, the antiangiogenic potential of the drug pair was assessed by its delivery to chick embryo. It is noteworthy that the nanocarrier did not record any adverse effect on parameters of angiogenesis implying its inert nature. Further embryos treated with dual paired drug loaded nanocarrier showed significant decrement in branching points and vessel density formed during angiogenesis **(figure 3.9 & 3.10)**. A pronounced decrease total vessel network length and segment numbers was also observed [73]. Growth factors such as FGF2 and VEGF induce endothelial cells to secrete proteases and plasminogen activators that degrade the vessel basement membrane, leading to cell invasion into the surrounding matrix and formation of new vessels **(figure 3.11).**

Hence, they hold the key to induce angiogenesis and have specially been implicated in cancerous tissues [56]. An up regulation of FGF2 and VEGF gene implicates in tumorigenesis. In selected drug pair dosed to the embryos, doxorubicin in combination with curcumin induces tumor regression via down regulation of above mentioned genes [42]. This is confirmed by decrease in the mRNA levels of FGF2 and VEGF in a dose dependent manner upon treatment with drug loaded nanocarrier.

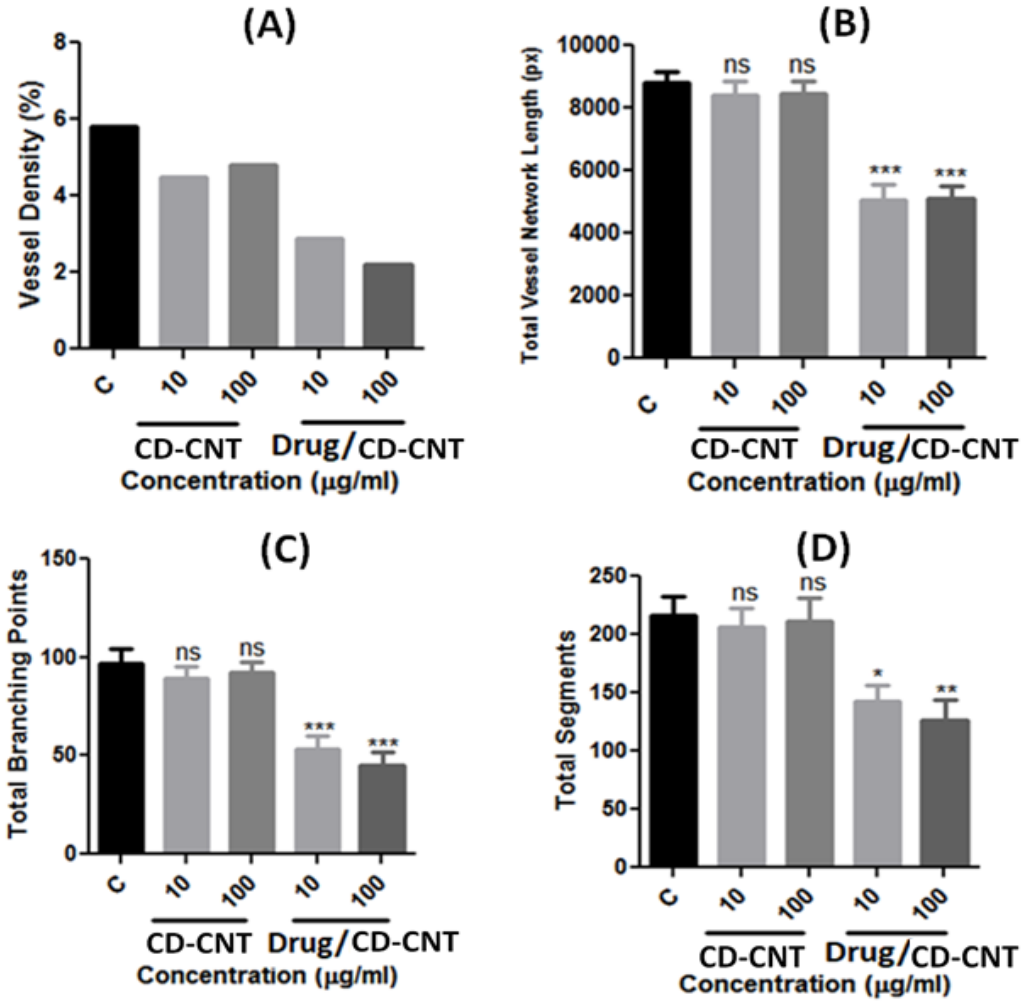


**Figure 3.9: Quantitative indices of angiogenesis in control and treated chick embryos (n=6 to 8 per group) after 4 h of treatment. A. Percentage vessel density, B. Total vessel network length, C. Total branching points of blood capillaries and D. Total segments of blood vessels. Values of B, C and D are represented as Mean ± SD; *p<0.05; **p<0.01 and *** p < 0.001)**

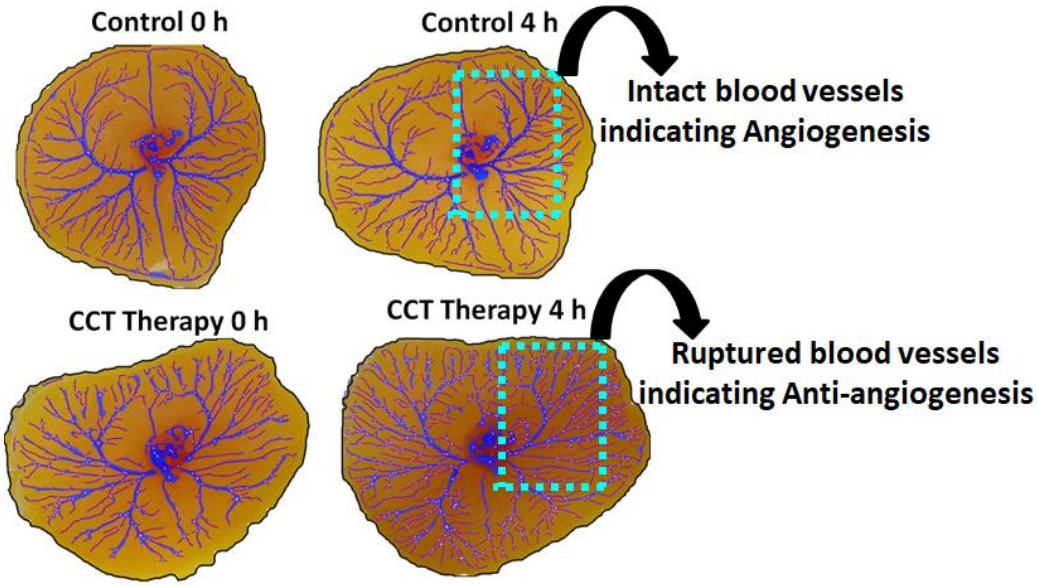


**Figure 3.10: Ex-ovo CAM Assay performed on Chick Embryo after treatment with DOX-CUR dual drug pair (CCT)**

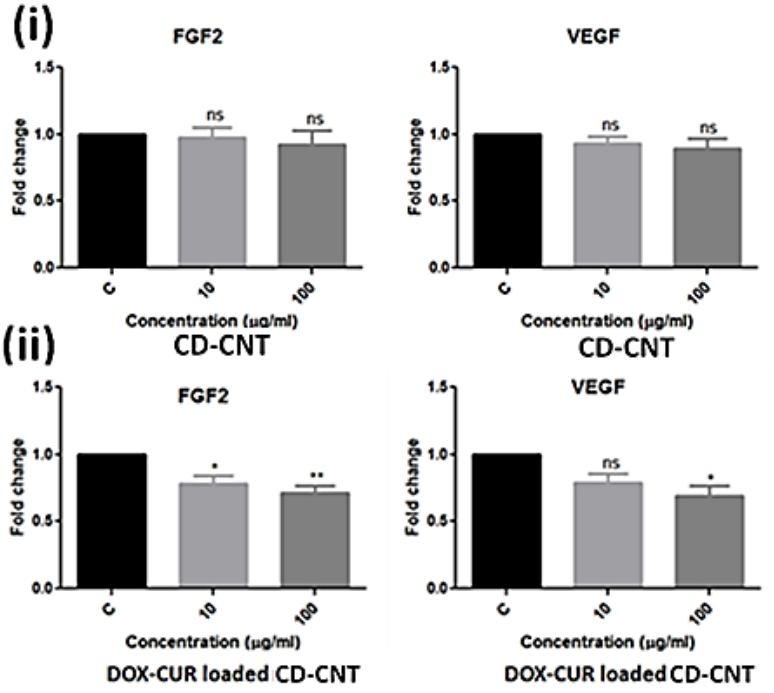


**Figure 3.11: mRNA levels of angiogenic genes FGF2 and VEGF following treatment to the chick embryo. The graphs shows the fold change in FGF2 and VEGF expression between control versus (i) nanocarrier (ii) drug pair loaded nanocarrier treated groups (n=6 chick embryo samples) Mean ± SD; ns non-significant, *p<0.05 and **p<0.01**

### 3.3.5 *In-vivo* Studies

The *in-vivo* studies were performed by the induction of Hepatocellular carcinoma (HCC) in the animals (Balbc mice model). Initially the in-vivo studies were attempted by administration of curcumin and DOX dual loaded carriers. However, for the drug concentration selected in our studies curcumin was not detected in the withdrawn blood samples or in the tissues even after 24 h in the control group.

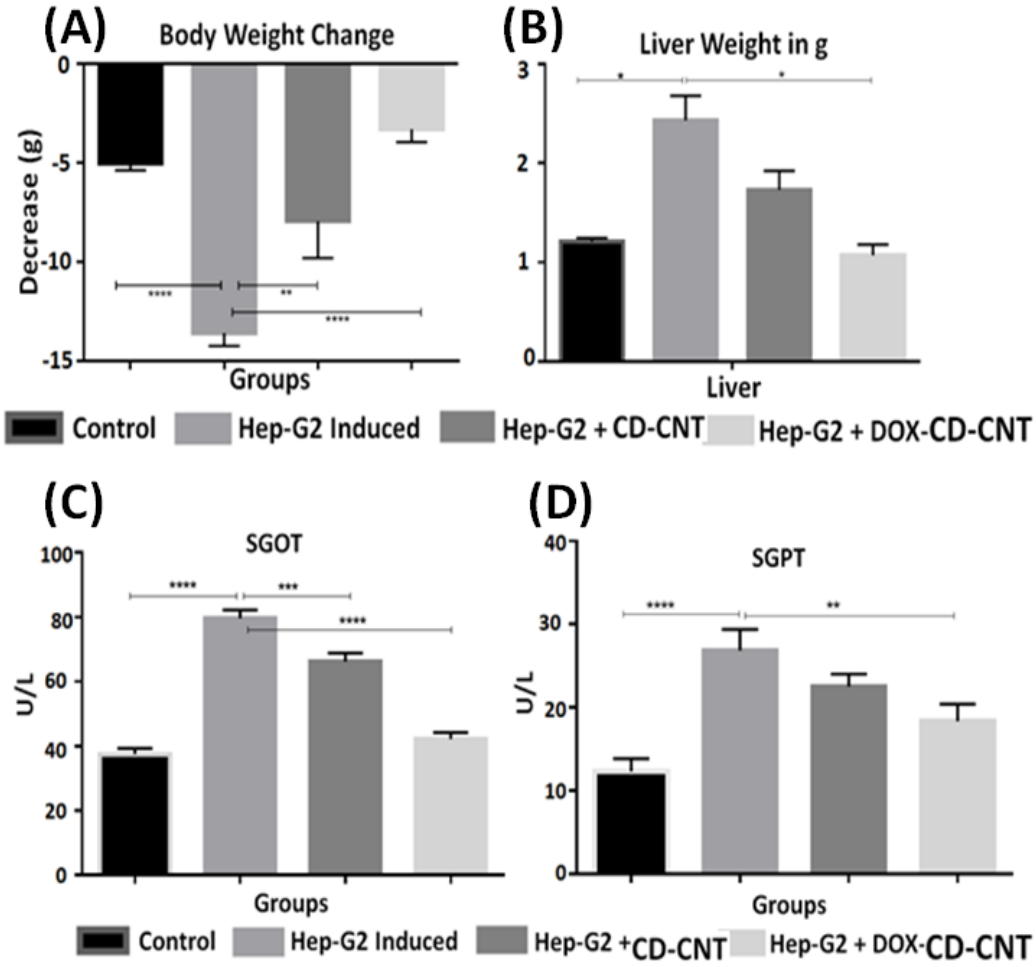


**Figure 3.12: (A) Changes in body weight, (B) weight of the liver and liver indices expressed in terms of (C) SGOT and (D) SGPT profile in the nude mice model under study. (n=4) under study the results are expressed as Mean ± SD *p<0.05; **p<0.01 and **** p < 0.0001**

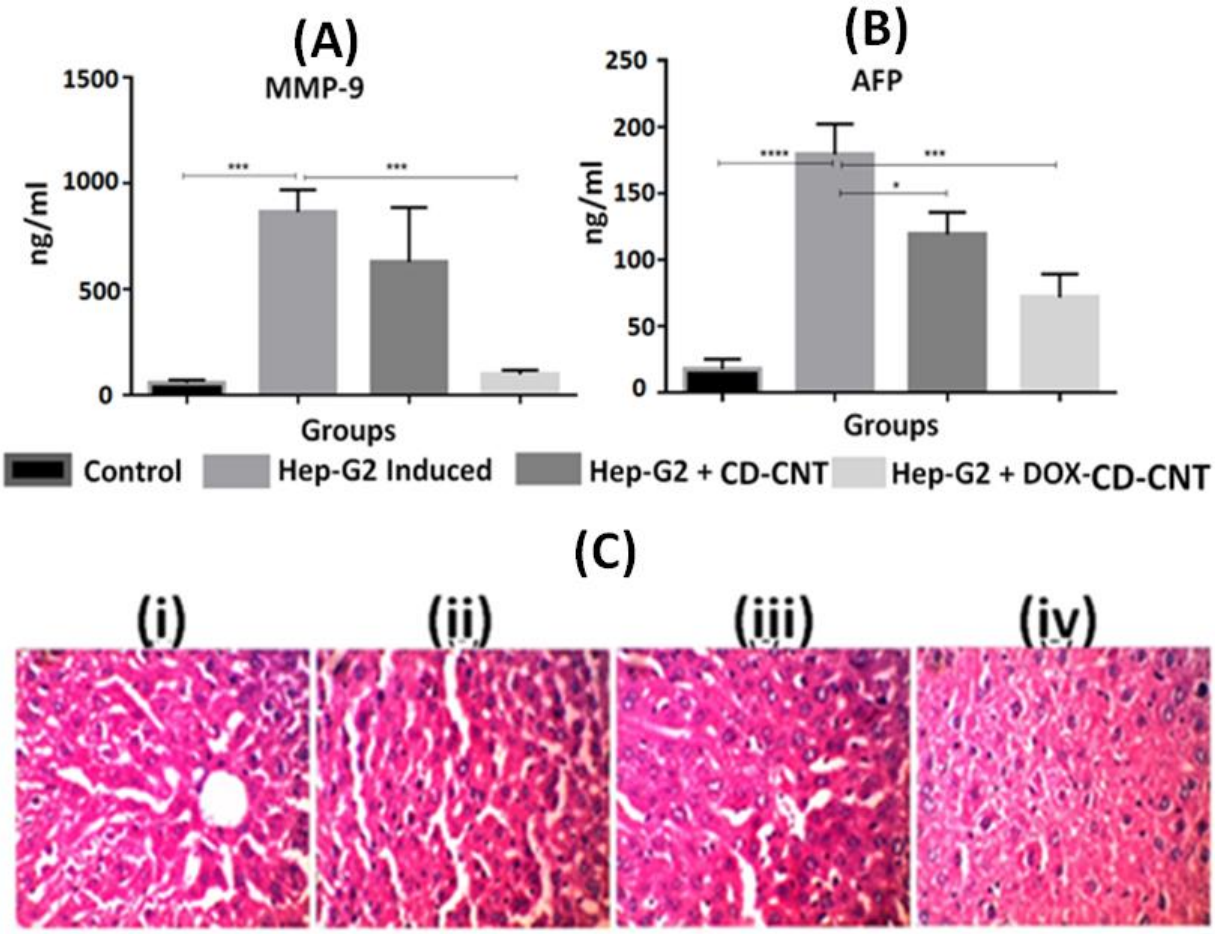


**Figure 3.13: (A) MMP-9 and (B) AFP levels in the animals (n=4) the results are expressed as Mean ± SD *p<0.05; ***p<0.001 and **** p < 0.0001 (C) Liver Sections of (i) Control and animals dosed with (ii) HEP-G2 (iii) HEP-G2+ nanocarrier (iv) HEP-G2+DOX loaded nanocarrier at 40X magnification.**

This may not be because of the failure of the carriers to deliver curcumin in vivo, since our observation is concomitant with the literature reports which mention absence of curcumin even at potentially high doses (440–2200 mg/day). They report that this may be because of further conversion of released curcumin into its metabolites in the blood [74]. Hence to assess the potential of nanocarriers, DOX.HCl loaded nanocarrier was selected for further in-vivo studies. The study of parameters like body weight and whole weight of the liver revealed a significant reduction of tumor after treatment with the drug loaded nanocarriers. Decrease in the body weight was observed in all the groups but the tumor induced group showed the most significant decline

**(figure 3.12A)**. As per the **figure 3.12B** the initial increase in weight of the liver are suggestive of tumor growth, which got reversed following treatment.

However, DOX loaded nanocarrier treated group did not show such an increase and the observed values were comparable to that of control. The liver function parameters as indicated (Serum SGPT and SGOT levels) showed a significant increment in HCC group. However the activity levels significantly diminished in those animals dosed with Dox loaded carriers. Thus a conclusion can be drawn that the liver functional indices were reinstated to normal levels after treatment **(Figure 3.12 C & D)**.

The HCC group showed elevated plasma levels of MMP-9 confirming onset and progression of hepatic tumor. On the contrary treatment with DOX loaded carriers caused a decrement MMP-9 levels **(figure 3.13A)**. AFP was found to be significantly elevated in the HCC induced group **(figure 3.13B).** Significantly lowered levels of AFP following treatment with DOX loaded CD-CNT suggests that nanocarriers are instrumental in targeted drug delivery.

There were evident alterations found in the histoarchitechture of liver that showed distorted liver lobes, de-arrangement of hepatic cod and canaliculi. This supports previous observations in HCC groups. This was supported by microscopic observations showing lesser extent of cellular de-arrangement in liver **(Figure 3.13C).** The distorted histoarchitechture was restored to near control morphology in the treatment groups. These results suggest that DOX induced prevention of tumor progression that is further enhanced by use of nanocarrier. These *in-vivo* studies thus conclude that the CD-CNT is efficacious for targeted drug delivery and cause a tumor regression.

### 3.4 Conclusion

To summarize, the synthesized formulations were explored for combinatorial therapy by encompassing multiple facets of cancer management. The nanocarrier were exhibited a pH – thermal dual responsive drug release of the dual drug pair DOX.HCl and curcumin synergistically. The nanocarrier showed a good drug entrapment efficiency of 92 %. A sustained release of both the drugs was observed over 30 h. An enhanced DOX.HCl release (90%) under conditions of tumor microenvironment whereas and elevated curcumin (85%) release at and pH 7.4 at elevated temperature. The release of drug was further found to be elevated upon exposure to NIR irradiation thus successfully exerting a photothermal effect. The cocktail chemotherapy and photothermal therapy were also found to work in synergism. The dual drug pair loaded

nanocarrier also demonstrated an anti-angiogenic potential as successfully demonstrated via CAM assay on chick embryo. A down-regulation of crucial growth factors (FGF2 and VEGF) was observed upon treatment with curcumin and DOX drug pair loaded CD-CNT. The stimuli responsiveness of the dual responsive polymer created a synergistic hostility in the tumor microenvironment and generating detrimental effect on tumor growth. *In-vitro* studies performed on HeLa and MCF-7 cells using drug loaded CD-CNT are in agreement with the observed drug release behavior; exhibiting cell mortality rate of 70% further increasing to 80% upon photothermal irradiation. The cancer induced Balbc mice demonstrated noteworthy decrement in the levels of cancer specific biomarkers MMP-9 and AFP indicating tumor regression which is also evident in histoarchitechture of the liver. Thus the injectable nanocarriers can be used to harness multiple facets of cancer therapy to enhance the therapeutic efficacy of drugs and assist MDR reversal.

.

**3.5 References**


1. Penny LK, Wallace HM. *Chem Soc Rev*. 2015: 8836–8847.
2. Liu Y, Zong Y, Yang Z, Luo M, Li G, Yingsa W, Cao Y, Xiao M, Kong T, He J, Liu X, Lei J. *ACS Sustain Chem Eng*. 2019; 7: 3614–3623.
3. Wang Y, Zhao R, Wang S, Liu Z, Tang R. *Biomaterials*. 2016; 75: 71–81.
4. Zhang P, Cheng F, Zhou R, Cao J, Li J, Burda C, Min Q, Zhu JJ. *Angew Chemie - Int Ed*. 2014; 53: 2371–2375.
5. Das M, Solanki A, Joshi A, Devkar R, Seshadri S, Thakore S. *Carbohydr Polym*. 2019; 206: 694–705.
6. Fabbro C, Ali-boucetta H, Ros D, Kostarelos K, Bianco A, Prato M, Ros T Da. *Chem Commun*. 2012: 3911–3926.
7. Wang J, Xu D, Deng T, Li Y, Xue L, Yan T, Huang D, Deng D. *ACS Appl Nano Mater*. 2018; 1: 1976–1984.
8. Yao X, Mu J, Zeng L, Lin J, Nie Z, Jiang X, Huang P. *Mater Horizons*. 2019; 6: 846–870.
9. de Sousa M, Visani de Luna LA, Fonseca LC, Giorgio S, Alves OL. *ACS Appl Nano Mater*. 2018; 1: 922–932.
10. Bafkary R, Khoee S. *RSC Adv*. 2016: 82553–82565.
11. Shi J, Kantoff PW, Wooster R, Farokhzad OC. *Nat Rev Cancer*. 2017; 17: 20–37.

12. Lee C, Kim H, Yu J, Yu SH, Ban S, Oh S, Jeong D, Im J, Baek MJ, Kim TH. *Eur J Med Chem*. 2017: 416–423.
13. Dong X, Sun Z, Wang X, Leng X. *Nanomedicine Nanotechnology, Biol Med*. 2017; 13: 2271–2280.
14. Dramou P, Fizir M, Taleb A, Itatahine A, Dahiru NS, Mehdi YA, Wei L, Zhang J, He H. *Carbohydr Polym*. 2018; 197: 117–127.
15. Shao L, Zhang R, Lu J, Zhao C, Deng X, Wu Y. *ACS Appl Mater Interfaces*. 2017; 9: 1226–1236.
16. Wang D, Wu S. *Langmuir*. 2016; 32: 632–636.
17. Du C, Ding Y, Qian J, Zhang R, Dong C-M. *J Mater Chem B*. 2019: 5306–5319.
18. Wang N, Feng Y, Zeng L, Zhao Z, Chen T. *ACS Appl Mater Interfaces*. 2015: 14933–14945.
19. Zhang L, Qin Y, Zhang Z, Fan F, Huang C, Lu L, Wang H, Jin X, Zhao H, Kong D, Wang C, Sun H, Leng X, Zhu D. *Acta Biomater*. 2018; 75: 371–385.
20. Bafkary R, Khoee S. *RSC Adv*. 2016; 6: 82553–82565.
21. Xie L, Wang G, Zhou H, Zhang F, Guo Z, Liu C, Zhang X, Zhu L. *Biomaterials*. 2016; 103: 219–228.
22. Permatasari FA, Fukazawa H, Ogi T, Iskandar F, Okuyama K. *ACS Appl Nano Mater*. 2018; 1: 2368–2375.
23. Peng X, Wang R, Wang T, Yang W, Wang H, Gu W, Ye L. *ACS Appl Mater Interfaces*. 2018; 10: 1084–1092.
24. Dinesh B, Schurhammer R, Collin D, Guilbaud-che C, Bianco A. *ACS Appl Mater Interfaces*. 2019: 13147–13157.
25. Wang Y, Barhoumi A, Tong R, Wang W, Ji T, Deng X, Li L, Lyon SA, Reznor G, Zurakowski D, Kohane DS. *Acta Biomater*. 2018; 72: 287–294.
26. Paik SR, Kim B. *Chem Mater*. 2017; 9: 3461−3476.
27. Kuo W, Chen H, Chen S, Chang C, Chen P, Hou Y, Shao Y, Kao H, Hsu CL, Chen Y, Chen S, Wu S, Wang J. *Biomaterials*. 2017; 120: 185–194.
28. Yao X, Tian Z, Liu J, Zhu Y, Hanagata N. *Langmuir*. 2016; 33: 591–599.
29. Cao Y, Dong H, Yang Z, Zhong X, Chen Y, Wenhao Dai, Zhang X. *ACS Appl Mater Interfaces*. 2016; 9: 159–166.

30. Feng Y, Li N, Yin H, Chen T, Yang Q, Wu M. *Mol Pharm*. 2018; 16: 422–436.
31. Tran TH, Nguyen HT, Pham TT. *ACS Appl Mater Interfaces*. 2015; 7: 28647–28655.
32. Cong Y, Xiao H, Xiong H, Wang Z, Ding J, Li C, Chen X, Liang X, Zhou D, Huang Y. *Adv Mater*. 2018; 30: 1706220–1706230.
33. Deshpande NU, Jayakannan M. *Biomacromolecules*. 2017; 18: 113–126.
34. Kao FH, Akhtar N, Chen CC, Chen HY, Thakur K, Chen YY, Chen C, Chattopadhyay S. *ACS Appl Bio Mater Biomater*. 2018: 533–543.
35. Wang H, Ke F, Mararenko A, Wei Z, Banerjee P, Zhou S. *Nanoscale*. 2014; 6: 7443–7452.
36. Bao X, Wang W, Wang C, Wang Y, Zhou J, Ding Y, Wang X, Jin Y. *Biomaterials*. 2014; 35: 8450–8466.
37. Wang J, Guo F, Yu M, Liu L, Tan F, Yan R, Li N. *J Control Release*. 2016; 237: 23–34.
38. Li X, Wu M, Pan L, Shi J. 2016: 93–105.
39. Heister E, Brunner EW, Dieckmann GR, Jurewicz I, Dalton AB. *ACS Appl Mater Interfaces*. 2013: 1870–1891.
40. Wang L, Li B, Xu F, Xu Z, Wei D, Feng Y, Wang Y, Jia D, Zhou Y. *Carbohydr Polym*. 2017; 174: 904–914.
41. Mejri A, Vardanega D, Tangour B, Gharbi T, Picaud F. *J Phys Chem B*. 2015: 604–611.
42. Bhattarai P, Hameed S, Dai Z. *Nanoscale*. 2018: 5393–5423.
43. Zhang W, Du F, He M, Bai L, Gu Y, Yang L, Liu Y. *Eur J Med Chem*. 2019: 390–400.
44. Ding X, Su Y, Wang C, Zhang F, Chen K, Wang Y, Li M, Wang W. *Appl Mater Interfaces*. 2017: 23353–23369.
45. Carmeliet P, Jain RK. *Nature*. 2000; 407: 249–257.
46. Zhang J, Li J, Shi Z, Yang Y, Xie X, Lee SMY, Wang Y, Leong KW, Chen M. *Acta Biomater*. 2017; 58: 349–364.
47. Yang YW, Sun YL, Song N. *Acc Chem Res*. 2014; 47: 1950–1960.
48. Solanki A, Das M, Thakore S. *Carbohydr Polym*. 2018; 181: 1003–1016.
49. Seidi F, Shamsabadi AA, Amini M, Shabanian M, Crespy D. *Polym Chem*. 2019; 10: 3674–3711.
50. Tungala K, Adhikary P, Azmeera V, Kumar K, Ramesh K, Krishnamoorthi S. *RSC Adv*. 2016; 6: 41594–41607.

51. Zhang P, Huang H, Huang J, Chen H, Wang J, Qiu K, Zhao D, Ji L, Chao H. *Appl Mater Interfaces*. 2015: 23278–23290.
52. Zheng Y, Wang L, Lu L, Wang Q, Benicewicz BC. *ACS Omega*. 2017; 2: 3399–3405.
53. Song X, Wen Y, Zhu J ling, Zhao F, Zhang ZX, Li J. *Biomacromolecules*. 2016; 17: 3957–3963.
54. Itatahine A, Mehdi YA, Fizir M, Man Q, Dramou P, He H. *New J Chem*. 2018: 1326–1336.
55. Pradhan P, Giri J, Rieken F, Koch C, Mykhaylyk O, Döblinger M, Banerjee R, Bahadur D, Plank C. *J Control Release*. 2010; 142: 108–121.
56. Murugesan S, Mousa SA, Connor LJO, Lincoln DW, Linhardt RJ. *FEBS Lett*. 2007: 1157–1160.
57. Patel S, Jana S, Chetty R, Thakore S, Singh M, Devkar R. *Sci Rep*. 2018: 1–11.
58. Datsyuk V, Kalyva M, Papagelis K, Parthenios J, Tasis D, Siokou A, Kallitsis I, Galiotis C. *Carbon N Y*. 2008: 833–840.
59. Yadav M, Das M, Savani C, Thakore S, Jadeja R. *ACS Omega*. 2019; 4: 11993–12003.
60. Han JK, Jeon DH, Cho SY, Kang SW, Yang SA, Bu SD, Myung S, Lim J, Choi M, Lee M, Lee MK. *Sci Rep*. 2016; 6: 1–8.
61. Gao C, Jin YZ, Kong H, Whitby RLD, Acquah SFA, Chen GY, Qian H, Hartschuh A, Silva SRP, Henley S, Fearon P, Kroto HW, Walton DRM. *J Phys Chem B*. 2005; 109: 11925–11932.
62. Isoda H, Furukawa Y. *J Phys Chem B*. 2015; 119: 14309–14314.
63. Meyns M, Primpke S, Gerdts G. *Anal Methods*. 2019; 11: 5195–5202.
64. Dong X, Sun Z, Wang X, Zhu D, Liu L, Dong X, Sun Z, Wang X, Zhu D, Liu L, Leng X. *Drug Deliv*. 2017: 143–151.
65. Wang H, Li J, Zhang X, Ouyang Z, Li Q, Su Z, Wei G, We. *RSC Adv*. 2013: 9304–9310.
66. Zhang Y, Sha R, Zhang L, Zhang W, Jin P, Xu W, Ding J, Lin J, Qian J, Yao G, Zhang R, Luo F, Zeng J, Cao J, Wen L ping. *Nat Commun*. 2018; 9.
67. Tabish TA, Zhang S, Winyard PG. *Redox Biol*. 2018; 15: 34–40.
68. Dohle DS, Pasa SD, Gustmann S, Laub M, Wissler JH, Jennissen HP, Dünker N. *J Vis Exp*. 2009: 1620–1626.
69. Wu H, Jin H, Wang C, Zhang Z, Ruan H, Sun L, Yang C, Li Y, Qin W, Wang C. *ACS*

*Appl Mater Interfaces*. 2017; 9: 9426–9436.

70. Datir SR, Das M, Singh RP, Jain S. *Bioconjug Chem*. 2012: 2201–2213.
71. Yan J, Xu X, Zhou J, Liu C, Zhang L, Wang D, Yang F, Zhang H. *ACS Appl Bio Mater*. 2020; 3: 1216–1225.
72. Badruddoza AZM, Rahman MT, Ghosh S, Hossain MZ, Shi J, Hidajat K, Uddin MS. *Carbohydr Polym*. 2013; 95: 449–457.
73. Chen H, Wang CS, Li M, Sanchez E, Li J, Berenson A, Wirtschafter E, Wang J, Shen J, Li Z, Bonavida B, Berenson JR. *Int J Oncol*. 2010: 71–79.
74. Shen L, Liu CC, An CY, Ji HF. *Sci Rep*. 2016; 6: 1–10.